Proceeding of the IEEE
International Conference on Robotics and Biomimetics
Dali, China, December 2019

Prediction of Liver Respiratory Motion Based on Machine Learning

Xuezhi Bao[1,2,*], Deqiang Xiao[1,2,*],Baochun He[1,2], Wenchao Gao[3], Junliang Wang[3#], Fucang Jia[1,2,4#]

***Abstract*—Hepatic respiratory movement has always been an important factor that affects the accuracy of liver interventional therapy. To improve the prediction accuracy of image-guided therapy, we proposed a liver breath prediction model that combines machine learning, surface point set sparse registration, and internal and external breath amplitude correlation. We used surface sparse point set registration to calculate the displacement vector field of the liver surface and the displacement vector field of a specified region of the abdominal surface. Using correlation analysis of the internal and external respiratory amplitudes, we selected the liver displacement vector field that is closest to the input respiratory signal as the optimal training data. A patient-specific model that combines local vector field optimization with abdominal surface similarity optimization was constructed by combining the liver surface and the abdominal surface after segmentation, and accurate motion prediction was realized based on principal component analysis (PCA). In an experiment on 7 patients, we adopted two experimental verification methods: (1) only one data collection stage and one cross-validation stage were used, and (2) the experimental data that were collected in the first stage were used as the training data set, and the experimental data that were collected in the second stage were used as the test data set. The prediction errors of the two methods were 0.35 ± 0.08 mm and 0.96 ± 0.40 mm, respectively. In this experiment, we combined surface sparse point set registration with an internal and external breath amplitude correlation method, which substantially improved the runtime and accuracy of the experiment compared with the traditional PCA method.**

***Index Terms*—respiratory motion, liver, prediction, correlation analysis**

I. INTRODUCTION

Respiratory motion compensation has always been a hot issue in liver intervention [1]. Many minimal invasion technologies in cancer treatment technology involve radiation therapy or interventional radiology. Computed tomography (CT) imaging techniques are used for adjuvant therapy because CT images contain accurate anatomical information and are of high signal-to-noise ratio and high resolution. Many issues must be considered during radiation therapy, such as changes in tumor shape and location, and other non-autonomous movements. Of the non-autonomous movements, the most readily observed is respiratory movement. Organ movements that are caused by respiratory motion, errors in structure and anatomy, and deformation of doses are all issues to be considered during radiation therapy. In response to these concerns, the current mainstream method is to use respiratory motion modeling to compensate for respiratory motion to accurately determine the displacement deformations of organs and tumors [2].

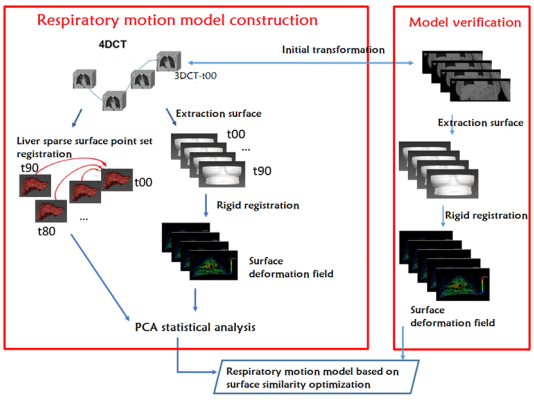

Figure 1. Respiratory motion model construction process.

Murphy et al. utilized a neural network for real-time spatiotemporal tracking of radiotherapy points during free breathing and demonstrated that a nonlinear neural network heuristic learning algorithm can be used to predict lung tumor movement during free breathing [3]. However, when patients exhibit irregular breathing patterns, although the liver motion can be predicted, the accuracy is much lower. To solve this problem, McClelland et al. suggested the use of a proxy respiratory motion model that can easily predict organ movement during acquisition/intervention[1]. The motion model describes the mathematical relationship between the surrogate signal and the internal motion data. The model is fitted to preoperative data, and the substitute signal is used to predict the

[1]Research Lab for Medical Imaging and Digital Surgery, Shenzhen Institutes of Advanced Technology, Chinese Academy of Sciences, Shenzhen, 518055, China
[2]Shenzhen College of Advanced Technology, University of Chinese Academy of Sciences, Shenzhen 518055, China
[3]Department of Radiation Therapy, The 5th Medical Center, Chinese People's Liberation Army General Hospital, Beijing 100039, China
[4]Shenzhen Key Laboratory of Minimally Invasive Surgical Robotics and System, Shenzhen Institutes of Advanced Technology, Chinese Academy of Sciences, Shenzhen 518055, China
*These authors contributed equally.
Corresponding author: Fucang Jia, PhD, Shenzhen Institutes of Advanced Technology, Chinese Academy of Sciences, Shenzhen, China. Email: fc.jia@siat.ac.cn; Tel: 86-755-86392213, Fax: 86-755-86392299; Junliang Wang, PhD, The 5th Medical Center, Chinese People's Liberation Army General Hospital. Email: wjl1000@tom.com.

978-1-7281-6321-5/19//$31.00 ©2019 IEEE

internal motion during intervention. However, the large computational burden of this approach will hinder its real-time clinical application. In this paper, we propose a respiratory motion model that is based on the principal component analysis (PCA) method; the flow is illustrated in Figure 1. For real-time performance, we propose a method of correlation between internal and external respiratory amplitudes. The training set selection process eliminates the need for all samples to be considered during training, which substantially shortens the training prediction time. We separate the human liver, extract the liver surface, and use the sparse surface point set to obtain the internal displacement field instead of using all internal points. In all experiments on 7 patients, we obtained satisfactory results.

II. MATERIALS AND METHODS

A. 4D-CT dataset

In this study, we used 4D CT data from 7 patients, which were obtained in two stages. Detailed information on the CT data is presented in Table 1.

B. Data preprocessing

Our experiment used 14 sets of abdominal 4D CT images from 7 patients. Each set of 4D CT images contained a complete respiratory motion cycle, and each cycle was divided into 10 respiratory phases, namely, each 4D CT image contained 10 3D CT images of the abdomen. For each abdominal CT image, we will perform abdominal surface segmentation, liver segmentation, liver surface point extraction and abdominal surface extraction. A detailed flow chart is shown in Figure 2.

Table 1 Abdominal 4D CT image resolutions (unit: mm) and image sizes

Patient	Image resolution	Volume size	Acquisition time
Patient 1	0.98×0.98×1.5	512×512×103×10	1
Patient 1	0.95×0.95×1.5	512×512×103×10	2
Patient 2	0.92×0.92×1.5	512×512×118×10	1
Patient 2	0.94×0.94×1.5	512×512×118×10	2
Patient 3	1.01×1.01×1.5	512×512×134×10	1
Patient 3	1.11×1.11×1.5	512×512×188×10	2
Patient 4	1.02×1.02×1.5	512×512×132×10	1
Patient 4	1.10×1.10×1.5	512×512×132×10	2
Patient 5	0.96×0.96×1.5	512×512×122×10	1
Patient 5	1.00×1.00×1.5	512×512×122×10	2
Patient 6	1.04×1.04×1.5	512×512×127×10	1
Patient 6	1.11×1.11×1.5	512×512×127×10	2
Patient 7	1.00×1.00×1.5	512×512×150×10	1
Patient 7	1.02×1.02×1.5	512×512×150×10	2

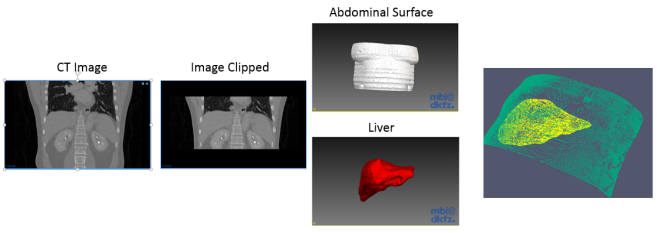

Figure 2. Data preprocessing

C. Surface point set sparse registration

For abdominal surface extraction, we performed region growing on the original CT image to obtain the abdominal region and to extract the entire abdominal surface [4]. Then, we extracted the upper surface of the abdomen according to the image pixel coordinate index by thresholding along the coronal direction. For liver surface extraction, we used the built-in program in MITK (http://www.mitk.org) for liver surface extraction. To increase the computational efficiency, we conducted sparse processing of the surface point set prior to registration and retained 30% of the point sets of the original surface. To construct the correspondence between the preoperative and intraoperative surface point sets, the extracted preoperative and intraoperative surfaces are projected into the same two-dimensional plane space to generate two-dimensional shape images (2D-shape-image), and these two two-dimensional shape images are registered to obtain the correspondence between the two surface point sets in the two-dimensional space. Finally, the three-dimensional spatial correspondence between the two surface point sets is established via back-projection. For the preoperative two-dimensional shape image, the preoperative abdominal CT surface is projected into its coronal plane to generate its two-dimensional projection image, and a binary image that contains a rectangular region is generated according to the region of interest (ROI) in the two-dimensional projection image. For the preoperative two-dimensional shape image, the process is similar to the step of generating a rectangular region using the centroid and the two distances with the intraoperative abdominal ROI pendulum. For the intraoperative two-dimensional shape image generation process, a squared ROI image is used to generate a rectangular area in the preoperative two-dimensional shape image space. The two distance values in the generation process of the rectangular area are expressed as pixel point indices. The distance is the physical distance instead of the pixel distance. Preoperative and intraoperative two-dimensional shape images are nonrigidly registered with scaling. After registration, the correspondence between the pixels of the ROI of the binary image can be determined. The correspondence between its coordinate space and the coordinate space of the two-dimensional image has been established, and the corresponding three-dimensional point set can be found from the two-dimensional pixel point coordinates by back-projection, thereby generating a corresponding point set between the preoperative and intraoperative surfaces. The initial rigid body registration of the preoperative and intraoperative surfaces was realized by a point-pair matching algorithm from the corresponding surface point set. Then, the initial registration was optimized using the classical iterative closest point (ICP) registration algorithm to realize the automatic registration of the abdominal and liver surfaces. A schematic diagram of surface sparse point set registration process is shown in Figure 3.

We chose to use the liver and abdomen surface images from the 3D CT images in the maximum respiratory state as reference images, and the liver and abdomen surface images of other phases were registered to the reference image using the sparse surface point set registration method. Via this approach, the respiratory motion deformation vector field (DVF) of each

respiratory phase relative to the reference phase with respect to the entire liver and abdomen is obtained.

D. Internal and external respiratory association

In the experiment, we calculated the amplitude of the DVF that was obtained after each phase registration and found that the change in the internal displacement vector field of the liver is approximately consistent with the change in the vector field of the abdominal surface displacement. The calculation results are presented in the figure 4 . For convenience, we present the calculation results for only 3 patients. We show the external respiratory changes in three patients over two phases. Since the magnitudes of the internal and external respiratory motion amplitudes are positively correlated, we evaluated them. The magnitude of the external respiratory motion amplitude was calculated from 7 data sets.

Algorithm implementation:

(1) The DVFs of 7 liver surfaces and the DVF of the abdominal surface were obtained by surface sparse point set registration, and the amplitude was calculated.

(2) The amplitude of liver movement and the amplitude of abdominal surface movement are correlated.

(3) From the data in the first stage, the nearest (best) two abdominal surfaces can be identified in the training data set based on the obtained abdominal surface motion. Then, the liver deformation displacement field that corresponds to the surface can be obtained.

(4) The two recently obtained liver DVF amplitudes are substituted as training samples. Thus, there is no need for a complete sample, which will save a substantial amount of time.

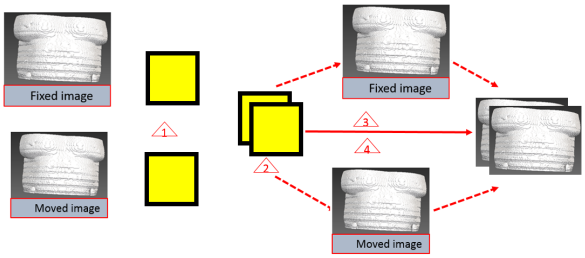

Figure 3 Schematic diagram of the surface sparse point set registration process

1: Projecting into a two-dimensional plane space for registration to obtain the correspondence between two surface point sets in two-dimensional space

2: Correspondence between two surface point sets in two-dimensional space

3: Back projection

4: Establishing a three-dimensional correspondence of surface point sets

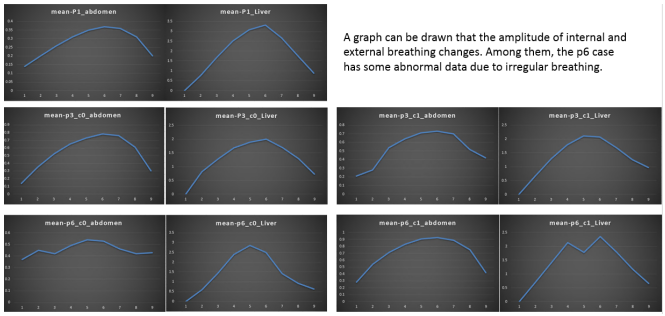

Figure 4 Statistics of the magnitudes of the internal and external respiration amplitudes for the first, third, and sixth cases were recorded.

E. PCA respiratory motion modeling

The construction process of the respiratory motion model that is based on the respiratory motion PCA statistical model, in combination with intraoperative surface similarity, is illustrated in Figure 5. The DVF that corresponds to each respiratory phase is represented as a separate column vector $u_j = [x_{1,j}, y_{1,j}, z_{1,j}, \dots . x_{M,j}, y_{M,j}, z_{M,j}]^T$, where $[x_{i,j}, y_{i,j}, z_{i,j}]^T$ represents the respiratory motion displacement vector at the j^{th} image pixel coordinate position of the abdominal image that corresponds to the i^{th} respiratory phase. The DVF that integrates the entire cycle constitutes the set U of the abdominal respiratory motion vector field U, where $U = [u_1, u_2, u_3, \dots, u_j, \dots, u_N]$. The matrix U is centered to obtain the matrix$\overline{U}$, and singular value decomposition is performed on $\overline{U}$ to obtain the eigenvectors and eigenvalues of the matrix$\overline{U}$. The eigenvalues are sorted from largest to smallest, and the eigenvectors that correspond to the two largest eigenvalues are used to construct a statistical model of the preoperative respiratory motion displacement field:

$$u(w) \approx \bar{u} + EW \qquad (1)$$

where u(w) represents the DVF that corresponds to any respiratory phase throughout the respiratory motion cycle; $\bar{u}$ represents the mean vector of the DVF for the entire respiratory cycle that was acquired prior to surgery; E represents a subset of the obtained set of feature vectors, namely, a matrix of the feature vectors that correspond to the largest two eigenvalues; W represents the PCA statistical model coefficient set; and the initial value is the corresponding feature value set.

Here, we will use the internal and external respiratory amplitude correlation method to construct the optimal training set; Hence, at this time, we use $\overline{u_{opt}}$ instead of $\bar{u}$. $\overline{u_{opt}}$ represents the average vector of the best training set that is obtained by the internal and external respiratory amplitude correlation method.

The abdominal surface area was extracted using the watershed method, in combination with a distance threshold, and the three-dimensional point cloud on the abdominal surface was reconstructed to obtain the intraoperative abdominal surface. The abdominal surface was extracted from the preoperative CT reference image using the thresholding method to obtain the preoperative abdominal surface. Based on the global shape two-dimensional projection method, the automatic rigid body registration of the intraoperative abdominal surface and the preoperative CT surface is realized. Then, an

optimization measure that is based on the nearest-neighbor point of the two surfaces with respect to the Euclidean distance is initialized:

$$W_{opt} = \arg max_W \mathrm{Sim}(S_W, S_i) \qquad (2)$$

where W_{opt} represents the optimal PCA statistical model parameters; S_W represents the surface from the CT of the abdomen that was obtained prior to surgery; S_i represents the intraoperative abdominal surface; and $Sim(S_W, S_i)$ represents the degree of similarity between the preoperative and intraoperative abdominal surfaces, which is inversely proportional to the Euclidean distance between the two surfaces. Then, the PCA statistical model parameters W were iteratively adjusted using the Levenberg-Marquart (LM) optimization algorithm. For each acquired model parameter, a DVF is calculated for the entire abdominal region. The DVF is applied to the preoperative CT reference image to obtain a deformed preoperative CT surface. Then, the similarity values of the two surfaces are updated. The iteration is terminated if the Euclidean distance between the two surfaces reaches the minimum value, namely, if the similarity measure is maximized, and the optimal PCA statistical model parameter W_{opt} is obtained. In turn, the internal respiratory field of the current breathing state is calculated:

$$u_{estimateed} = \overline{u_{opt}} + EW_{OPT} \qquad (3)$$

where $u_{estimateed}$ denotes the estimated vector field of the internal respiratory motion displacement throughout the abdomen.

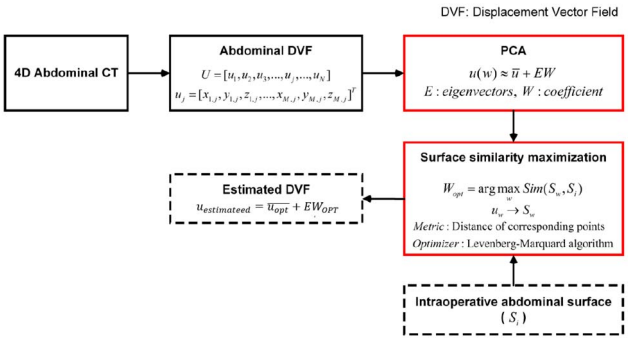

Figure 5 Respiratory motion modeling framework that is based on a respiratory motion PCA statistical model, in combination with the abdominal surface similarity

III. EXPERIMENTAL RESULTS

A. Motion model evaluation

The experiment used 7 sets of patient data, and each patient dataset was collected in two stages. We use the mean absolute error (MAE) and the model runtime to evaluate the performance of the model. We compared our experimental results with the experimental results of Fayad et al. [6], and another which were reported by Bao et al. [7].

B. Single-cycle data

The abdomen 4D CT images that were acquired in the first phase of each case contained 10 respiratory phases. The reference phase was removed, and the model was subjected to nine rounds of cross-validation using CT data that corresponded to the remaining nine respiratory phases, namely, a set of 4D CTs can be used to calculate 9 respiratory motion estimation errors. The processing flow for each set of 4D CT images is as follows: First, each preprocessed image is subjected to abdominal segmentation and surface extraction. Then, the reference respiratory phase is selected, and the respiratory motion vector field of the residual phase is calculated for the abdominal CT image with respect to the reference phase (DVF) calculation. Next, the test phase is selected from the 9 respiratory stages, the respiratory motion model is constructed using the remaining 8 DVFs, and the simulated surface is used to calculate the DVF in the current state that corresponds to the abdominal surface of the simulated surface as the model input. The DVF calculates the motion estimation error of the model via comparison with the DVF that corresponds to the test phase. Nine error calculations were generated from the repeated test phases of the nine breathing phases.

For each calculation of the motion estimation error, the median of the difference vector between the estimated abdominal DVF and the corresponding ground-truth DVF is regarded as a result of a single error calculation. The 70 motion estimation errors of the 7 sets of 4D CT images, along with the mean, standard deviation, and median values of the statistical errors, were calculated. The experimental results for 7 sets of patient data are presented in Figure 6. The results of our experiments and the experimental results of Bao et al. are presented in Table 2.

Table 2 Statistical results of the motion estimation errors of the respiratory motion models for single motion estimation (Unit: mm)

Method	Mean	SD	Median
PCA_BE	1.52	0.41	1.24
Fayad et al.,2011	2.76	0.82	1.34
Our method	0.95	0.38	0.85

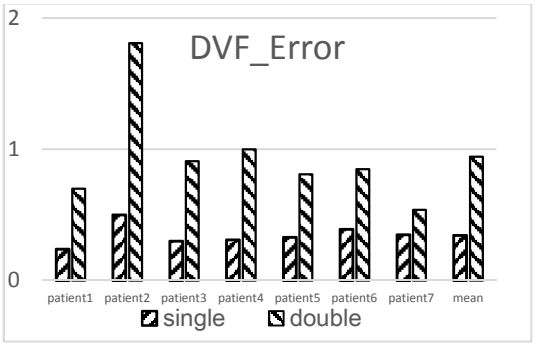

Figure 6 Average errors that were calculated using the single-motion and double-motion data for seven patients (unit: mm)

C. Double-cycle data

Our respiratory motion model was trained in the first phase and evaluated on the data that were acquired in the second phase. Here, for each motion estimation error calculation, the median of the difference vector between the estimated abdomen DVF

and the corresponding ground-truth DVF is regarded as a result of a single error calculation. The mean, standard deviation, and median values of the statistical error are presented in Figure 2, and the results of the comparative experiments are presented in Table 3.

Table 3 Statistical results of the motion estimation errors of the respiratory motion models for double motion estimation (Unit: mm)

Method	Mean	SD	Median
PCA_BE	0.57	0.06	0.60
Fayad et al.,2011	0.67	0.04	0.64
Our method	0.35	0.08	0.33

D. Model runtime

In the experiment, we separately calculated the runtimes for the new method and the PCA_BE method on the same case, which are listed in Table 4. Due to the use of sparse surface point set registration and internal and external respiratory amplitude correlation methods in the experiment, the runtime of our new method is substantially shorter.

Table 4 Statistical results of the model runtime for the same patient (Unit: ms)

Method	Phase 1	Phase 2	Phase 3	Phase 4	Phase 5	Phase 6	Phase 7	Phase 8	Phase 9	mean
PCA_BE	43083	56354	51003	58240	63834	74173	68190	61836	51039	58639.11
Our method	44	44	33	49	49	47	46	49	47	45.33

IV. CONCLUSIONS AND DISCUSSION

In this paper, a method for liver respiratory motion compensation that is based on surface sparse point set registration and an internal and external respiratory amplitude correlation method is proposed. It realizes more accurate motion compensation than our original method. The surface sparse point set registration method realizes large improvements in terms of the registration accuracy, and the calculation efficiency is substantially increased. In addition, our newly proposed internal and external respiratory amplitude correlation method plays a highly important role in constructing the model. Obtaining the most relevant displacement vector field for training not only reduces the calculational burden of the model but also shortens the model prediction time, thereby making our model more suitable for clinical application.

The proposed modeling framework, which is based on a PCA statistical motion model, in combination with abdominal surface similarity, for constructing the respiratory motion model is more suitable for the modeling of traditional respiratory motion via the application of phase divergence data. During human breathing, breathing patterns change[8] and during each cycle[9], breathing movements "lag". The abdominal surface movement also changes when the abdominal surface respiratory motion changes during surgery. Divergence data are generated during the application phase of the model (instead of the training phase). Due to the movement displacement that is caused by respiratory movement, the motions of the abdominal surface and the internal organs of the abdomen are correlated; however, there is no strict one-to-one correspondence. The correlation between visceral respiratory movement and exercise is linear, and polynomial or B-spline methods[10] are used to describe the internal and external associations. The PCA-based respiratory motion statistical model is more comprehensive than the traditional method, and it accurately describes the relationship between the surface and body movements. The patient's abdominal surface is acquired in real time as the current respiratory state agent, and the target is adjusted via the statistical model parameters. The model parameters are optimized to estimate the current internal respiratory motion displacement. Finally, the statistical motion model is realized via the parameter solution process. The application phase is scalable, which avoids the need to assume stable internal and external relationships as in traditional model construction. Therefore, compared with traditional methods[11], the statistical motion model is more robust in combination with the intra-abdominal abdominal surface similarity modeling framework. For the preoperative PCA statistical motion model that is based on the abdominal DVF[12], the eigenvectors that correspond to the two largest eigenvalues are used to construct a statistical model. This is because when using PCA to extract the principal component of the sample space[13], the sum of the two largest eigenvalues constitutes more than 80% of the sum of all eigenvalues, namely, the eigenvectors that correspond to the two largest eigenvalues can approximately reconstruct all of the original sample variables. Since only two feature vectors are used for the construction of the PCA statistical model, the parameters of the preoperative statistical motion model are the two coefficient terms of the PCA model. The abdominal surface deformation that is caused by respiratory motion is relatively small, and when applied, the automatic abdominal surface registration algorithm does not fail due to the respiratory motion.

However, the same problem is encountered with our method as with the previously proposed method: The model is constructed for a single case. The application of the model to the population will render the constructed respiratory motion model more clinically meaningful. Our future work will focus on this.

ACKNOWLEDGMENTS

This work was supported in part by Shenzhen Key Basic Science Program (JCYJ20170413162213765 and JCYJ20180507182437217), the Shenzhen Key Laboratory Program (ZDSYS201707271637577), the NSFC-Shenzhen Union Program (U1613221), and the National Key Research and Development Program (2017YFC0110903). The authors do not disclose conflicts of interest.

References

[1] J.R. McClelland, D.J. Hawkes, T. Schaeffter, et al. Respiratory motion models: A review. Med. Image Anal.,17(1): 19-42, 2013.

[2] A. Fassi, J. Schaerer, M. Fernandes, et al. Tumor tracking method based on a deformable 4D CT breathing motion model driven by an external surface surrogate. Int. J. Radiat. Oncol. Biol. Phys., 88(1): 182-188, 2014.
[3] M.J. Murphy. Using neural networks to predict breathing motion. Seventh International Conference on Machine Learning and Applications, San Diego, CA, USA. 528-532, 2008.
[4] D. Xiao, Q. Hu, F. Jia. Statistical motion modeling with surface similarity maximization for respiration compensation in thoraco-abdominal radiotherapy. Int. J. Comput. Assist. Radio. Surg. 12 (S1): S42–S43, 2017
[5] R. Li, J.H. Lewis, X. Jia, et al. On a PCA-based lung motion model. Phys. Med. Biol., 56(18): 6009-6030, 2011.
[6] H. Fayad, T. Pan, O. Pradier, et al. Patient specific respiratory motion modeling using a 3D patient's external surface. Med. Phys., 39(6): 3386-3395. 2012.
[7] X.Z. Bao, W.C. Gao, D.Q. Xiao, et al. Bayesian model-based respiration motion prediction for liver: using single-cycle and double-cycle 4D CT images. 2019 International Conference on Medical Imaging Physics and Engineering. Shenzhen, China. 2019.
[8] V. Blanz, T. Vetter. Face recognition based on fitting a 3D morphable model. IEEE Trans. Pattern Anal. Mach. Intell., 25(9): 1063-1074. 2003.
[9] J.W.H., Wolthaus, J.J. Sonke, M. van Herk, et al. Reconstruction of a time-averaged midposition CT scan for radiotherapy planning of lung cancer patients using deformable registration. Med. Phys., 35(9): 3998-4011. 2008.
[10] A. Fassi, M. Seregni, M. Riboldi, et al. Surrogate-driven deformable motion model for organ motion tracking in particle radiation therapy. Phys. Med. Biol., 60(4): 1565-1582. 2015.
[11] J.R. McClelland, S. Hughes, M. Modat, et al. Inter-fraction variations in respiratory motion models. Phys. Med. Biol., 56(1): 251-272. 2011.
[12] F. Ernst, R. Bruder, A. Schlaefer, et al. Correlation between external and internal respiratory motion: a validation study. Int. J. Comput. Assist. Radiol. Surg., 7(3): 483-492. 2012.
[13] H. Fayad, T. Pan, J.F. Clement, et al. Technical note: Correlation of respiratory motion between external patient surfac1e and internal anatomical landmarks. Med. Phys., 38(6): 3157-3164. 2011.